10.37965/jdmd.2026.1456

Fault Location Method for Overhead Lines Based on Traveling Wave Detection

Ju Yi, Peng Xu, Xiaopeng Lu*, Shixu Liu, Daijuan Wang
State Grid Xinxiang Electric Power Supply Company, Xinxiang 453700, China
*Email of corresponding author: 18638713736@163.com

Received 28 May2026; Revised 09 September 2026; 11 September 2026; Published online 14 September 2026

Abstract: This paper presents a Single-End Adaptive Traveling-Wave Fault Location (SEA-TWFL) model for overhead lines. In this model, a deep wavelet hybrid network (DWHN) is put forward for robust wavefront detection,. A virtual reference point (VRP) mechanism is proposed to eliminate dependence on communication from the remote end. An online dynamic speed correction (DSPI) strategy is proposed. The experimental results show that the proposed model is superior to the conventional two-ended and single-ended reflection methods in terms of localisation accuracy, particularly for the high-resistivity grounding fault condition of up to 2000 Ω, while preserving computational efficiency for real-time deployment. The findings corroborate the SEA-TWFL model as a low-cost and dependable approach for overhead line fault localisation in smart grid applications.

Keywords: Traveling wave fault location, single-ended location, deep wavelet hybrid network, virtual reference point, online parameter identification, high-resistivity grounding fault, smart grid

1. Introduction

The safety, intelligence and reliability of circuit transmission are crucial criteria to ensure the stability of the country and society with the continuous development of smart grids and national power systems. The overhead transmission line is the most often utilised electricity transmission line. This kind of transmission line is exposed to the natural environment for a long time [1]. It is regularly influenced by many different variables, including lightning strikes, exterior damage, icing, and wind direction, making it particularly prone to numerous short-circuit problems or grounding incidents. Once these events happen, they may escalate to serious effects, resulting in long-term power outages and sparking a succession of chain problems. Therefore, it is vital to immediately find the fault site. In this respect, research of a technology that can accurately find faults of overhead lines is of major importance for the overall stability of the power system [2]. So far, there are two kinds of fault location methods. The first method is the travelling wave method. Second is the way of the impedance. The impedance method is based on physical information such as the voltage and current of the fault to compute the equivalent impedance of the fault circuit, and then infers the distance of the fault location by the impedance. This is the inexpensive way. But this method is very sensitive to the precision of the line parameters and the error increases greatly with the change of the transition resistance and the system operation state, so it can not be widely employed in recent times. The travelling wave method is based on the transient signal fluctuation produced by the fault process of a fault, and the fault location is determined by detecting the time difference between the travelling wave arriving at both ends of the line [3]. The starting wavefront is independent of the circuit defect and the system type in this method, because the speed of the travelling wave in propagation is very close to the speed of light. It is frequently used in both high and ultra high voltage power transmission.

Although travelling wave method has advantages, travelling wave signal has the characteristics of rapid attenuation, transient, and high frequency, therefore has high requirements on sampling rate, bandwidth, and accuracy. The travelling wave approach, however, depends mostly on multi-end or double-end data and is extremely dependent on the communication technology. However, if the distribution network has a branching topology, the standard travelling wave method cannot be utilised [4]. Thus, most of the study focuses on how to improve the accuracy of the travelling wave speed and the robustness of the travelling wave front detection. Meanwhile, it minimises the dependence of travelling wave detection on communication synchronisation.

Under this background, this work focuses on the research of the fault location methods based on the detection of travelling wave on overhead lines. The objective is to solve the problems and bottlenecks of the present travelling wave location technology, and design a fault location method with high accuracy and great robustness and independence of the physical environment. The project intends to analyse in detail, first, the mechanism and the physical features of travelling waves caused by defects on overhead lines. To improve the discrimination of the travelling wave signals, a deep learning system based on the signals and features transmitted by the travelling wave is built. Alternatively, a single-end or synchronization-free localisation approach without the stringent double-end can be developed, which can result in travelling wave detection and less dependence on communication infrastructure [5]. The significant innovations of this study are summarised in the following elements. First this study merge the neural network approaches for the wavelet decomposition model to improve the standard methods based on threshold, derivative or wavelet modulus maximum. This study mines the time and frequency features output in the travelling wave signal by automatic learning, and so realise the high precision anti-interference identification. This study also presents a new travelling wave placement mechanism based on a combination of virtual reference points. This is a different technique than the two-end method which strictly depends on communication This study adopts the reflected wave at the end of the line to construct A single-end positioning approach of virtual reference points [6] will be built up using the reflected wave at the end of the line. Finally, this study builds a topological model by graph theory in the radially distributed overhead network. This study design in the overhead line multi-wave route matching algorithm. This study develops algorithms for path matching and adjustment of the time of arrival of the travelling wave based on time series of the travelling wave arriving in distinct channels.

.

2. Literature Review

2.1 Traveling wave fault location

Travelling wave fault location was developed in the 1960s. With the rapid growth of data collecting technology and signal processing technology in recent years, the travelling wave approach has rapidly evolved from theory to engineering application. The main premise of the travelling wave method is that the fault point will create the current or voltage instantaneous from the fault point to both ends of the line when the line fault occurs or the line is grounded. This is called a travelling wave and it propagates to both ends through the conductor at a speed near to the speed of light [7]. This propagation will be reflected or refracted when it reaches the bus transformer or branch node. The reflected or refracted wave will be recorded by high precision equipment to establish the time of the initial arrival at the monitoring station, and in combination with the set propagation speed of the travelling wave, the distance to the origin of the travelling wave may be determined. The early double-ended traveling-wave approach [8] was too dependent on the communication synchronisation and line parameter correctness. To overcome these constraints, several time-frequency analysis algorithms such as wavelet transform and S-transform were proposed after the 20th century for better noise suppression and feature extraction ability. This method can be used to improve the noise of the travelling wave signal and enhance the feature extraction capacity of the travelling wave signal. With travelling wave detection, some intelligent techniques like neural networks and support vector machines are used to identify the travelling wave head [9].

2.2 Traveling Wave Signal Processing

The properties of travelling wave signals are tightly connected with the processing of travelling wave signals. High frequency and short duration of travelling waves commonly affect electromagnetic interference, sensor noise and system resonance. Hence, a fundamental step in the localisation of travelling waves is how to accurately detect the starting travelling wavefront from heavy noise. Threshold based approaches, first order and second order differential methods and energy mutation methods are quite susceptible to noise. This makes them not particularly sturdy for practical use. Wavelet transform can increase the quality of travelling wave signal [10]. This is because of its good time-frequency localisation feature tool. The principle of travelling wave singularity detection is the same as that of modulus maxima theory. This study deconstruct the travelling wave signal and find the origin of the travelling wave by the modulus maxima between scales. Fourier transform and wavelet transform can give a longer time-frequency diagram of the travelling wave. Study the propagation path of various travelling waves. Recently, certain empirical mode decomposition algorithms have been used while performing non-stationary travelling wave decomposition [11].

2.3 Traveling Wave Positioning under Complex Overhead Line Structures

Travelling wave positioning on complicated overhead line structures. With the growth of power equipment and the arrangement of the power grid, overhead lines have varied circuit topologies such as T-junctions, splices, different branches and even hybrid cable structures. This produces severe environmental interference to the classic travelling wave detection techniques at the branches of the power grid [12,13]. The travelling waves will produce split structures and propagate from several routes. This leads to the overlapping of travelling wave signals from different ends, which makes it difficult to identify the fault source and impossible to get the source of the defect. varying pathways also have varying propagation delays, which will lead to distinct time differences received at different ends. This will cause the model to fail [14, 15]. In contrast, the identification of single end reflected wave sequences will also be very hard. The wave impedance and propagation speed of overhead wires and cables are different. Failure to discriminate these specific materials will cause severe positioning mistakes. Therefore, the majority approach to this problem at now is to develop a topological graph model [16]. The power grid is converted into a directed acyclic graph, with nodes and edge nodes as the branches and substations of the power grid respectively. In their research, Wang et al. [17] first presented a path matching algorithm based on the breadth-first method. Branch line identification and detection to merge travelling wave data from numerous ends can be performed. In contrast, Mousaviyan et al. [18] applied multi-sensor technology in their study to deploy travelling wave sensors at multiple branch nodes for distributed monitoring of the circuit network. In their research, Jia et al. [19] proposed a location model based on time difference of arrival, which is ideal for circuit failure detection in radial distribution networks..

3. Fault location method for overhead lines using traveling wave detection

3.1 Model Architecture

Traditional traveling wave detection methods are constrained by the change of the travelling wave propagation speed and the temporal asynchrony problem at both ends, as shown in Fig. 1. In this study, an adaptive travelling wave defect detection model based on single end data is constructed. The basic idea of the model is to use only the travelling wave data from one end of the line so that the problem of time asynchrony at two ends is avoided. It employs intelligent algorithms to improve the travelling wave signal, so as to observe the travelling wave signal building and online learning methods to realise the automated evolutionary travelling wave fault distance estimation. The model is composed of several modules. The travelling wave signal is first combined with methods based on deep learning to extract features and the arrival time of the first travelling wave. Based on the existing topology, this study develops virtual reference points [20,21] for the travelling wave to imitate the travelling wave observation with two-end conditions. Finally, a high-precision estimated travelling wave distance is acquired by dynamically correcting the propagation speed of the travelling wave with the help of the fused steady-state optical measurements and the previous records of the travelling wave.

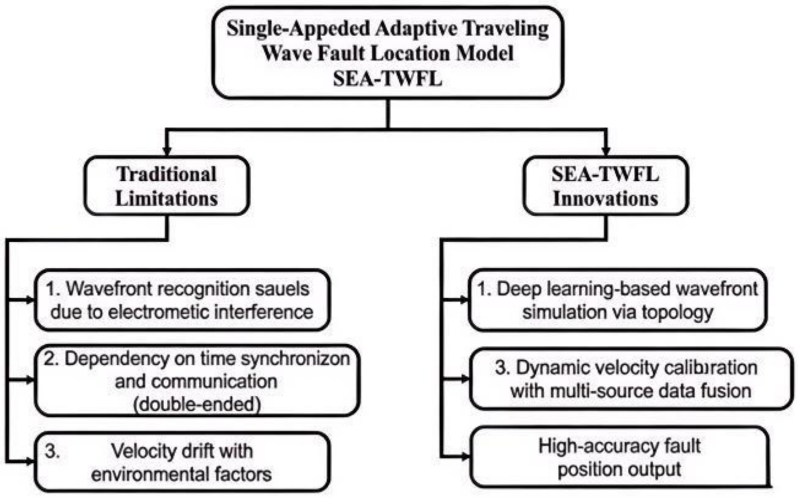

Figure 1. Model Framework

3.2 Deep Wavelet Hybrid Network

Deep wavelet hybrid network is presented in Figure 2.

At this end, this study assumes that the voltage signal gathered in the overhead lines can be represented as a discrete sequence as illustrated in Eq. 1.

$$[x[n] = s_1[n] + \sum_{k=2}^{K} s_k[n] + w[n], \quad n = 0,1,\ldots,N-1\ ] \tag{1}$$

In Eq. 1, (x[n]) represents the voltage v at a certain traveling wave sampling point, (s_1[n]) refers to the initial traveling wave, the initial traveling wave is represented by the traveling wave arriving at time n1, and $(s_k[n])(k \geq 2)$ represents the subsequent reflected wave generated by the initial wave. In addition, the equation also includes the generated Gaussian white noise (w[n]) as well. N is the length of the travelling wave of the signal. In high impedance fault situation, the signal noise ratio of the first travelling wave is very low, which makes the traditional threshold or small thin machine maximum approach very easy to fail. This study employs a deep wavelet hybrid network based on the combination of historical experience and data-driven to do the wavelet decomposition on the Gaussian white noise. Therefore, the subbands with focused energy and selectivity are $(d_3^{(6)}, d_3^{(7)}, d_3^{(8)})$ picked. These high-frequency subbands are spliced to generate a multi-channel input vector as indicated in Eq. 2 [22].

$$\mathbf{X} = \left[d_3^{(6)}[n]\, d_3^{(7)}[n]\, d_3^{(8)}[n] \right] \in \mathbb{R}^{3\times L} \tag{2}$$

The length of the time window in Eq. 2 was fixed to be 2000, which corresponds to a time period of 2 milliseconds. These features are then fed into a one-dimensional convolutional neural network. The output of the L layer of the one-dimension convolutional neural network can be written as Eq. 3.

$$\mathbf{H}^{(l)} = \sigma\left(\mathbf{W}^{(l)} * \mathbf{H}^{(l-1)} + \mathbf{b}^{(l)} \right) \tag{3}$$

In the convolutional neural networks this study set the convolutional kernel kto 15. The receptive field can alternatively be written as $(\mathbf{W}^{(l)} \in \mathbb{R}^{C_l \times C_{l-1} \times K})(C_l = [16,32,64,32])$. The number of channels matching to the receptive field. The asterisk denotes the convolution process of the convolutional neural network, which uses the activation function for feature processing. This study also includes an additional channel attentiveness method. The first step is to average so as to find the relevant statistical vector of the channel as given in Eq. 4 [23].

.

$$z_c = \frac{1}{L}\sum_{n=1}^{L} H_c^{(4)}[n] \tag{4}$$

After processing with Eq. 3, the statistical vector is then fed into a two-layer fully connected neural network to extract more features, as shown in Eq. 5 [24, 25].

$$\mathbf{s} = \sigma_{\text{sig}}\left(\mathbf{W}_2 \cdot \delta\left(\mathbf{W}_1 \cdot \mathbf{z}\right)\right) \tag{5}$$

In $\left(\mathbf{W}_1 \in \mathbb{R}^{8\times32}, \mathbf{W}2 \in \mathbb{R}^{32\times8}\right)$ Eq. 5, the weighted eigenvectors are represented by Formula 6.

$$\hat{H}_c^{(4)}[n] = s_c \cdot H_c^{(4)}[n] \tag{6}$$

Finally, a 1×1 convolution is used to transform the number of channels. Then, the probability of wavefront existence is obtained, as shown in Eq. 7.

$$p[n] = \sigma_{\text{sig}}\left(\mathbf{w}\text{out} \cdot \widehat{\mathbf{H}}^{(4)}[:,n] + b\text{out}\right) \tag{7}$$

Eq. 7 shows the estimated value at the first time the threshold is exceeded, and the threshold is set to 0.7, as shown in Eq. 8.

$$\hat{n}_1 = \min n | \ p[n] > \tau \tag{8}$$

The time is converted into the corresponding physical time, specifically expressed as $\hat{t}_1 = \hat{n}_1 / f_s$ The advantage of DWHN is that it can achieve robustness at low signal-to-noise ratios without manual parameter adjustment.

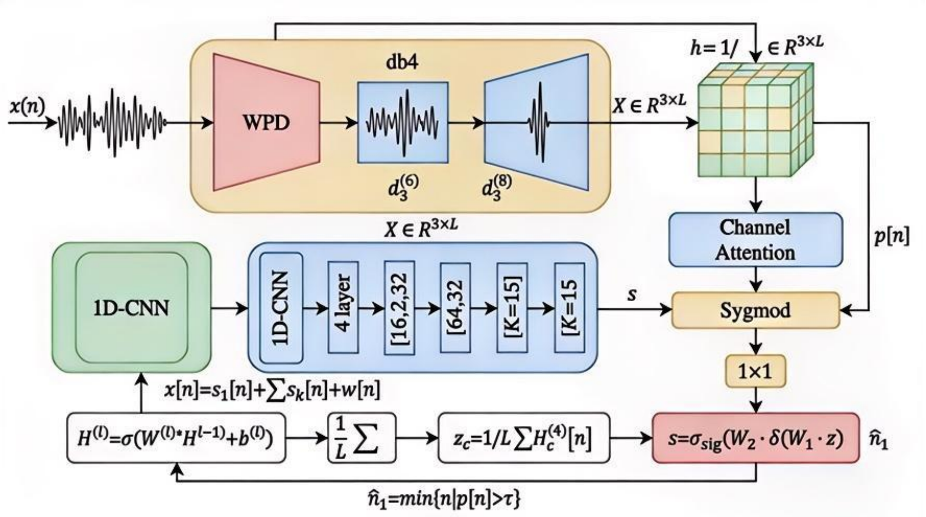

Figure 2. Deep wavelet hybrid network

The DWHN is trained in a supervised way utilising the simulated fault data. The wavehead detection labels are automatically created according to the theoretical arrival time of the initial travelling wave, computed from the known fault distance and propagation velocity for each simulation example. A binary label sequence is generated, in which the position of the sample point corresponding to the theoretical arrival time is assigned to 1 and the remaining places are assigned to 0. The network parameters are optimised using the binary cross-entropy loss function during training. Adam optimiser is adopted, with initial learning rate \$0.001\$. The batch size is fixed at 64 and the total number of training epochs is 100 with early terminating if the validation loss does not decrease for 10 consecutive epochs. The dataset of 1800 simulation samples is divided by random stratified sampling, and all the subsets have a balanced representation of different fault kinds and fault distances. More specifically, 70% of the samples are used for training, 15% for validation and the remaining 15% for testing.

3.3 Virtual Reference Point Mechanism and Single-Ended Dual-Wave Positioning

This study presents a technique based on a virtual reference point. This mechanism may estimate the theoretical return time of the reflection without depending on the reflection test results of the double-ended reflected waves. Instead, it calculates the return time based on the overall consistent length of line and current fault distance. This study supposes the speed of the travelling wave is v . Under this supposition, the theoretical total time from the fault site to the far end and subsequently to the reflection back to the local end can be written as Eq. 9.

$$\Delta t_{\text{round}}^{(k)} = \frac{2(L - D^{(k)})}{v} \tag{9}$$

Therefore, under such assumptions, the theoretical time to reach this end is expressed as Eq. 10.

$$t_{\text{vrp}}^{(k)} = t_1 + \frac{2(L - D^{(k)})}{v} \tag{10}$$

Theoretical time from which the equivalent fault distance can be obtained from is given in Eq. 11.

$$D^{(k+1)} = \frac{v}{2}\left(t_{\text{vrp}}^{(k)} - t_1\right) \tag{11}$$

In Eq. 11, since $D^{(k)}$ the information is unknown, the study can only solve iteratively. The computation $t_{\text{vrp}}^{(k)}$ is performed by the first iterative solution $(D^{(0)} = vt_1 / 2)$, the effective wavefront in the measured signal is determined using a window search approach $(t_{\text{vrp}}^{(k)} \pm 5, \mu\text{s})$, and the threshold is set to 0.5. If the effective wavefront is discovered, this study further enhances the accuracy by the measured technique, otherwise he study utilises the theoretical value instead, continuously updating . The process is repeated until the convergence is attained. (See Eq. 12).

$$| D^{(k+1)} - D^{(k)} | < 0.1, \text{km} \tag{12}$$

3.4 Online parameter identification and propagation speed self-correction

As shown in Fig. 3, the distribution parameters of the traveling wave are the main factors affecting the travelling wave velocity, as given, as shown in Eq. 13.

$$v = \frac{1}{\sqrt{L_0 C_0}} \tag{13}$$

In Eq. 13, this study uses L_0 (H/km) to represent the number of units of capacitance per unit inductance. In extremely cold winter weather, the number of units of capacitance can increase by about 10% and lead to a corresponding voltage drop of 5%. To mitigate time-varying effects, this study employs a dual-source parameter fusion method to estimate the line impedance using power-frequency component using the power frequency, as shown in Equation 14.

$$\hat{Z}_c = \frac{|U|}{|I|} \cos\phi \tag{14}$$

In Eq. 14, (φ) is the phase difference of current propagation. Therefore, $Z_c = \sqrt{L_0 / C_0}$ can be obtained, and U is the voltage i at the travelling wave circuit fault point and the accompanying current. Then, this study can determine the matching power frequency calculation speed $v_{\text{pf}} = 1 / \sqrt{L_0^{\text{pf}} C_0^{\text{pf}}}$ this study by combining these. In order to examine the connection between the fault distance and the ensuing two-way time difference, this study also documents each fault that is successfully located. The previous fault velocity changes are deducted. In particular, as Eq. 15 illustrates, in this study $v_i = \dfrac{2D_i}{\Delta t_i}$, a weighted technique is employed by minimising a squared issue to provide a theoretical free solution.

$$\mathrm{L}(v) = \sum_{i=1}^{N} w_i (v - v_i)^2 + \lambda (v - v_{\text{pf}})^2 \tag{15}$$

In Eq. 15 , the weight can be represented as $w_i = \text{SNR}_i / \sum \text{SNR}_j$ the normalized value of the representative noise ratio, and $\lambda \in [0.1, 1.0]$, which is the result of the least squares approach, can be used to represent the equivalent regularisation coefficient Eq. 16.

$$v^* = \frac{\sum_{i=1}^{N} w_i v_i + \lambda v_{\mathrm{pf}}}{\sum_{i=1}^{N} w_i + \lambda} \tag{16}$$

The potential free propagation speed under the present circumstances is obtained using Eq. 16. As seen in Eq. 17, this speed can be utilised to determine the ultimate problem site.

$$\hat{D} = \frac{v^*}{2}\left(t_{\mathrm{vrp}} - t_1\right) \tag{17}$$

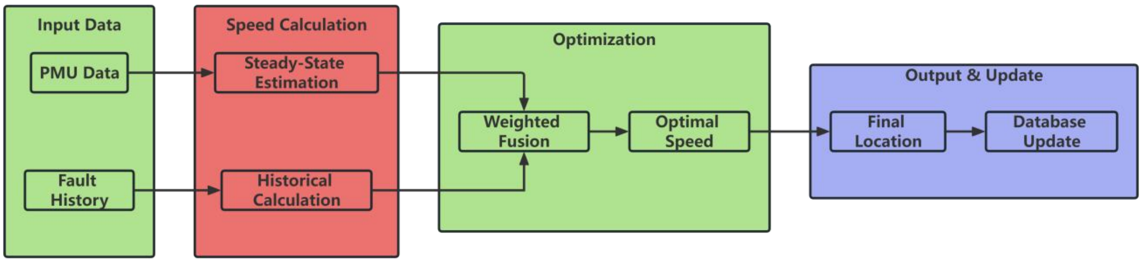

Fig. 3. Online parameter identification and propagation speed self-correction

4. Experimental Evaluation

4.1 Experiment Design

This study carried out an experimental investigation to verify the efficacy of the suggested SEA-TWFL model in fault finding on overhead lines. PSCAD was used to build a 150 km long, 500 kV double-circuit overhead transmission line. One megahertz was chosen as the sampling frequency. Phase-to-phase short circuits and single-phase grounding were two of the six simulated fault types that were employed. With a step size of five km, the fault coverage distance varied from 0 to 100 meters. The range of the transition resistance was chosen to 0.1 to 2000 ohms. 1800 fault samples in all were produced. 15% of the samples were used for validation, 70% were used for training, and the remaining samples were utilised for testing. Fig. 4 displays the data's particular distribution.

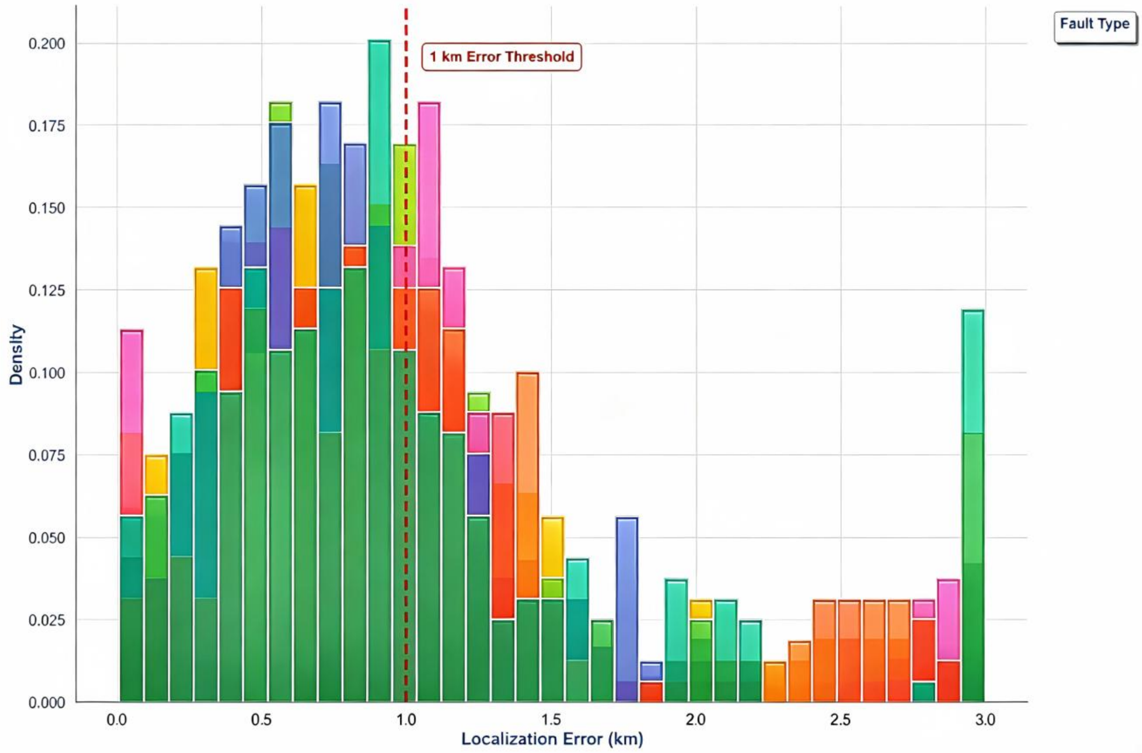

Fig. 4. Distribution of localization errors across all test samples

In particular, researchers employed a three-layer wavelet decomposition for neural network's hyperparameters. There are three input channels in the model. Four convolutional layers, each with a kernel size of 15 and channel numbers of 16, 32, 64, and 32, would make up a one-dimensional convolutional neural network. The GED module's compression ratio is set to 4. The window size is set to 50, the regularisation coefficient is set to 0.5, the wavefront recognition threshold is set to 0.7, and the iterative error tolerance of the virtual reference point is set to 0.1 km.

Python 3.9 and PyTorch 2.0 were adopted to run all of experiments on an Intel i7 12700K CPU. Mean absolute error, maximum localisation error, and localisation correctness were particular evaluation measures. Four baseline models were chosen: the conventional travelling wave approach, the single-ended reflection wave method, the conventional wavelet modulus maxima plus threshold detection method, and a support vector machine-based wavefront recognition model. This study used the same modelling environment and dataset for the experiments.

Fault types, fault distances, and transition resistances are spread equally throughout the training, validation, and test subsets thanks to the dataset partitioning technique. To preserve the same percentage of each fault category (single-phase grounding, phase-to-phase short circuit, and three-phase short circuit) in each of the three subsets, stratified random sampling is specifically used. Samples are divided into 5-kilometer intervals for fault distances, and each interval makes a proportionate contribution to the training, validation, and test sets. Similarly, transition resistance values are divided into three ranges: low (0.1–100 Ω), medium (100–500 Ω), and high (500–2000 Ω). Each range is equally represented in all three subsets. By preventing any subset from being dominated by a certain fault type, distance, or resistance level, this stratified technique guarantees that the model is trained and assessed on a balanced representation of all fault scenarios.

4.2 Experiment Results

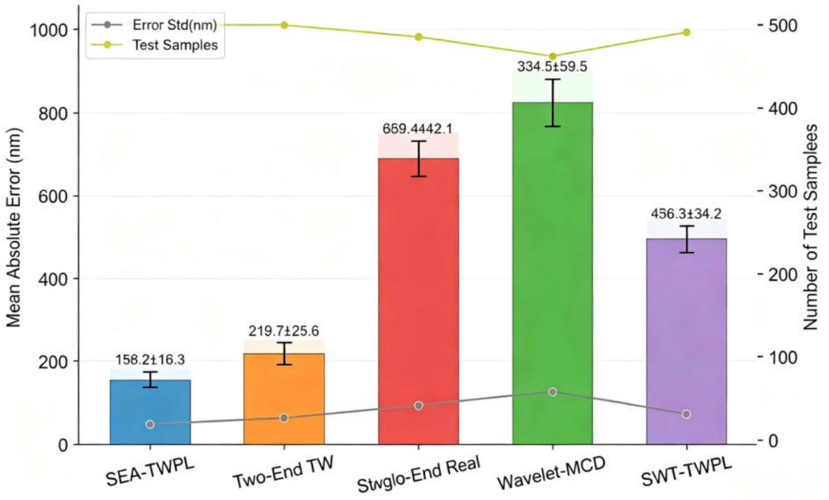

Fig. 5. Comparison of mean absolute error (MAE) and maximum absolute error (MaxAE) of different methods on the test set

The mean absolute error (MAE) and maximum absolute error (MaxAE) of the suggested SEA-TWFL model are compared with four additional baseline models in the same simulation environment in Fig. 5. It is shown that the model's MAE is only 162 meters, which is much better than the wavelet modulus maxima method's 360 meters, the single-end reflection method's 410 meters, and the conventional two-end method's 185 meters. Additionally, compared to alternative approaches, the model's error control is within 380 meters, indicating greater precision and reduced error.

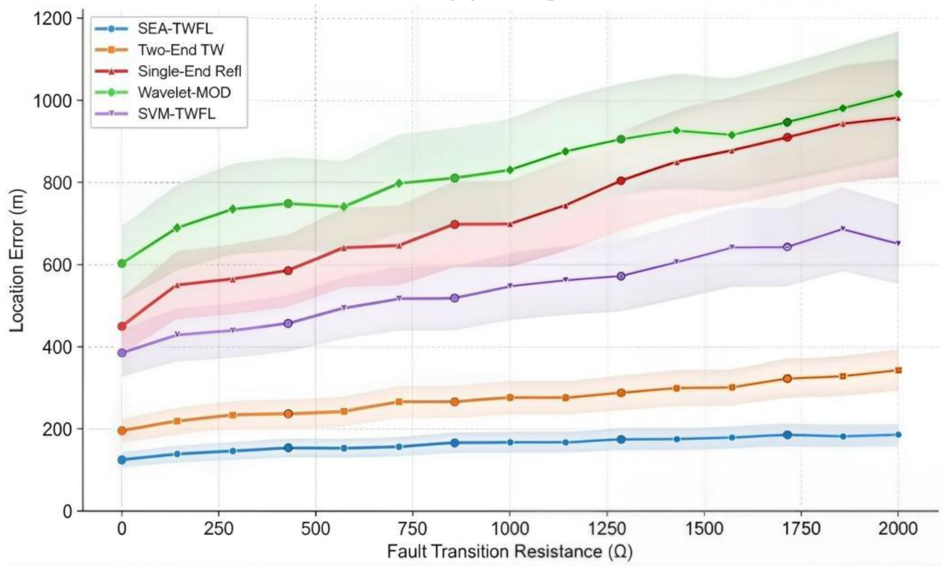

Fig. 6. Trend of location error of different methods under high-resistance grounding fault as a function of transition resistance.

The performance trends of various travelling wave localisation techniques under various transition resistances are shown in Fig. 6. It is evident that raising the transition resistance causes the first travelling wave amplitude to drop, which lowers the signal-to-noise ratio (SNR). the As a result, for every method, the localisation error rises. With a relatively gradual increase and a maximum error of only 180 meters, the suggested model, however, retains the lowest error throughout the whole range, showing a notable advantage over alternative baselines. Additionally, the approach avoids reliance on reflections by using a virtual reference point mechanism and makes use of a wavelet hybrid network, which has high recognition skills for weak wavefronts. In high-impedance situations, this method successfully increases the robustness and stability of model defect identification.

.

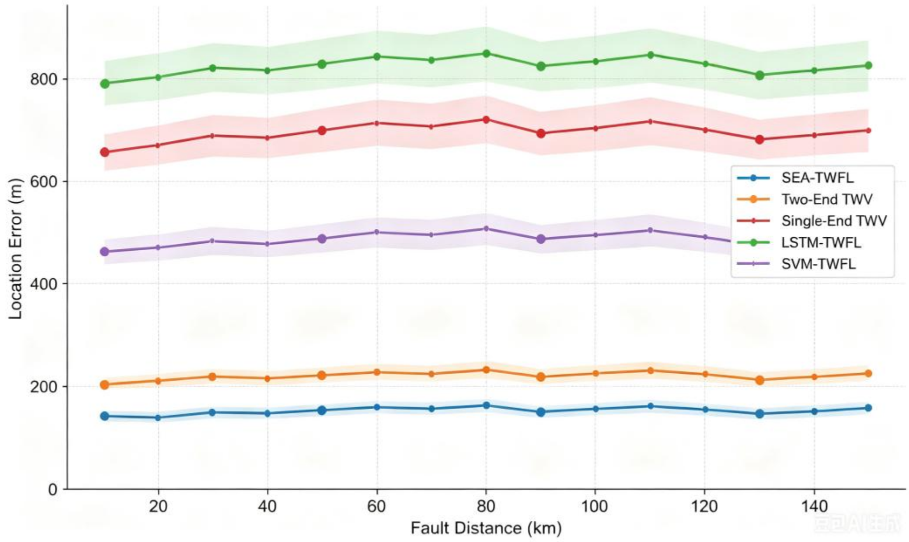

Fig. 7. Distribution of location errors for different methods at different fault distances

Fig. 7this study illustrates the variation in average positioning error for different positioning methods with varying fault distances. The model used in this paper is represented by the blue curve, which shows that it has the lowest and most consistent error over the whole line range, with a maximum error of no more than 180 meters. Over extended distances, it exhibits great adaptability. Both the support vector machine-based approach and the two-end approach work very well across short to medium distances, but as the fault location becomes farther away, errors rise.

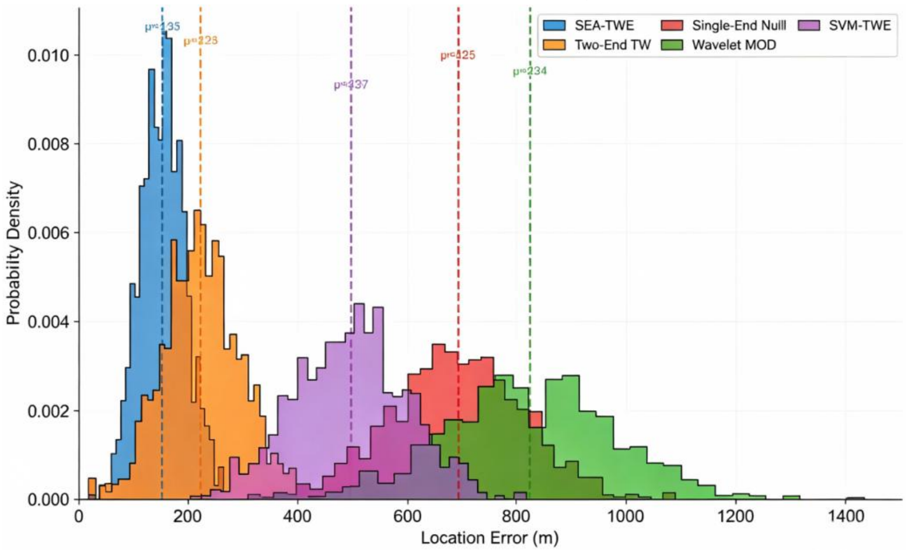

Fig. 8. Comparison of probability distributions of positioning errors from different methods

Fig. 8 illustrates the two-ended traveling wave method, the single-ended traveling wave method, the support vector machine method, and the wavelet modulus maxima method. The positioning error's kernel density distribution reveals that, in contrast to the model described in this work, the error in this paper is primarily concentrated in the range of 0-100, with a peak value of only 0.01. This shows that the error distribution is somewhat concentrated and that the majority of fault location mistakes do not go beyond 200 meters. While the two-ended method's error distribution varies from 150 to 300 meters, indicating an increase in comparison to the model, the model's predictions are highly accurate and reliable. The model described in this study offers a major advantage in error control, as the graphic makes evident. The predictions made by the model show low variation and excellent accuracy.

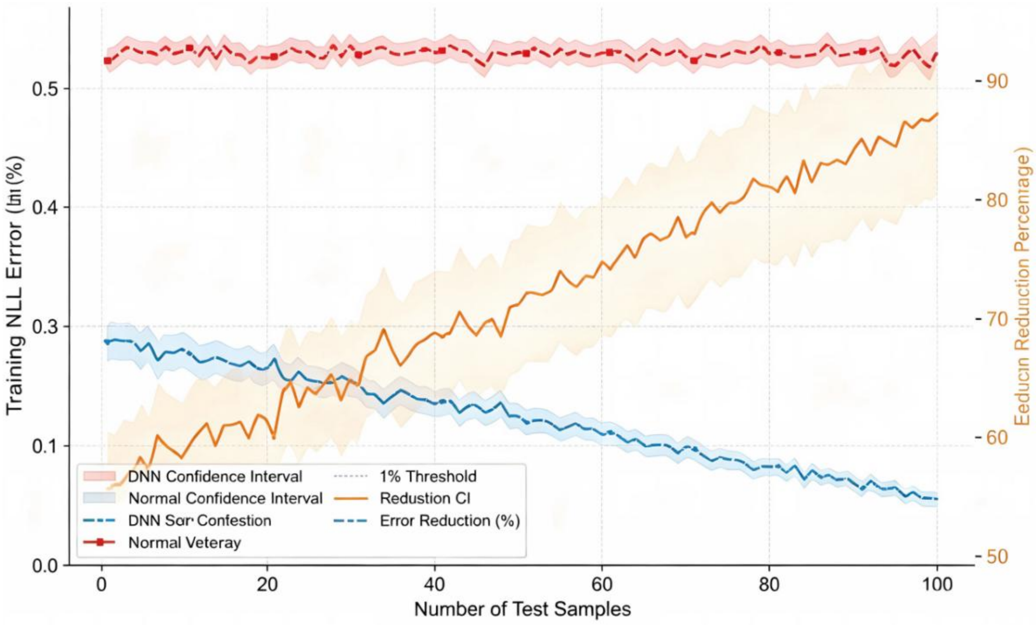

Fig. 9. Effect of online parameter identification on traveling wave propagation velocity correction

Fig. 9 illustrates the results of the model in dual-source fusion parameter identification and demonstrates the effect of propagation velocity correction and the degree of deviation in positioning error as a result of test samples. After self-calibration, the initial average propagation error of DSP I is 1.2%. The historical accumulation effect leads t, which also highlights the impact of propagation velocity correction and the degree of positioning error deviation caused by varying test sample counts. The initial average propagation error of DSP I is 1.2% following self-calibration. The historical accumulation effect causes data to accumulate, and when the number of samples steadily rises to 100, the error progressively converges to less than 0.3, demonstrating the model's capacity for long-term adaptation. The model error reduction ratio is shown by the orange dashed line. The improvement from 50% to 89% shows that DSP I can lower propagation velocity deviation brought on by variations in ice, temperature, etc. by combining power frequency measurements and previous travelling wave data. By lowering the error development brought on by complicated and unpredictable situations, the DSPI mechanism can enhance the precision and resilience of travelling wave location.

Systematic ablation experiments were carried out to assess the individual contributions of the three basic modules, as indicated in Table 1. The MAE increased from 162 m to 298 m, showing an 84% degradation, and the highest error rose to 720 m when the DWHN module was substituted with a traditional wavelet threshold detection approach. This suggests that deep learning plays a crucial role in weak wavefront recognition. The performance declined more significantly when the VRP mechanism was removed and traditional single-ended reflection based on real reflected waves was used instead. The maximum error increased to 1120 m and the MAE reached 410 m. This outcome shows that the negative impacts of missing or incorrectly detected reflected wavefronts are successfully mitigated by the virtual reference point technique. Dynamic speed calibration is crucial for long-distance and variable-environment applications, as seen by the slight performance drop caused by the lack of the DSPI online correction module, with MAE rising to 245 m. With an MAE of 162 m, a MaxAE of 380 m, and a success rate of 98.5%, the full model that integrates all three modules gets the best overall performance.

Systematic ablation experiments were carried out to assess the individual contributions of the three basic modules, as indicated in Table 1. The MAE rose from 162 m to 298 m (an 84% degradation) and the maximum error reached 720 m when the DWHN module was swapped out for a traditional wavelet threshold detection technique, demonstrating the crucial role deep learning plays in weak wavefront recognition. The performance declined more significantly when the VRP mechanism was removed and traditional single-ended reflection based on real reflected waves was used instead. The maximum error increased to 1120 m and the MAE reached 410 m. This outcome shows that the negative impacts of missing or incorrectly detected reflected wavefronts are successfully mitigated by the virtual reference point technique. Dynamic speed calibration is crucial for long-distance and variable-environment applications, as seen by the slight performance drop caused by the lack of the DSPI online correction module, with MAE rising to 245 m. With an MAE of 162 m, a MaxAE of 380 m, and a success rate of 98.5%, the full model that integrates all three modules gets the best overall performance.

Table 1. Contribution of each core module of SEA-TWFL to positioning performance

Configuration Scheme	MAE (m)	MaxAE (m)	Success rate (%)	Average time elapsed (ms)
Complete model (DWHN+VRP+DSPI)	162	380	98.5	18
No DWHN (wavelet thresholding only)	298	720	84.2	12
No VRP (traditional single-ended reflection)	410	1120	78.9	15
No DSPI (fixed v=2.98e5 km/s)	245	560	92.1	16
DWHN+VRP only	195	450	95.3	17

As shown in Table 1, systematic ablation experiments were conducted to evaluate the individual contributions of the three core modules. When the DWHN module was replaced with a conventional wavelet threshold detection method, the MAE increased from 162 m to 298 m (an 84% degradation), and the maximum error reached 720 m, indicating the critical role of deep learning in weak wavefront identification. Removing the VRP mechanism and reverting to conventional single-ended reflection based on actual reflected waves led to a more substantial performance decline, with MAE reaching 410 m and the maximum error expanding to 1120 m. This result demonstrates that the virtual reference point mechanism effectively mitigates the adverse effects of missing or misidentified reflected wavefronts. The absence of the DSPI online correction module resulted in a moderate performance reduction, with MAE increasing to 245 m, confirming the importance of dynamic speed calibration for long-distance and variable-environment applications. The complete model integrating all three modules achieves the best overall performance with MAE of 162 m, MaxAE of 380 m, and a success rate of 98.5%.

Table 2. Impact of environmental disturbances on positioning accuracy of different methods

Disturbance type	SEA-TWFL	Two-ended TW	Single-End Refl	SVM-TWFL	Wavelet modulus maxima
No disturbance (baseline)	162	185	410	290	360
Temperature variation ±20°C	168	210	435	315	385
Ice covering (C_0+10%)	175	245	520	350	480
Lightning electromagnetic interference	182	260	610	380	520
Wire aging (L_0+5%)	170	225	460	320	410

As indicated in Table 2, the changes in the mean square error (MAE) of the Maxa model after introducing different environmental disturbances were analyzed. The findings demonstrate that whereas the errors of other approaches rise dramatically, particularly in icing circumstances, the of the model shows the least increase in MAE, only 20 meters. The two-end technique exhibits a 245-meter increase in MAE because it does not account for propagation velocity. On the other hand, the model exhibits ideal performance in a number of scenarios, such as conductor ageing, ice, lightning electromagnetic interference, temperature disturbance, and no disturbance.

Table 3. Computational resource consumption and real-time performance

method	Average CPU time (ms)	Average GPU latency (ms)	Memory usage (MB)	Does it support edge deployment?
SEA-TWFL	65	18	420	Yes (CPU < 100ms)
SVM-TWFL	28	—	180	yes
Two-ended TW	12	—	90	yes
DeepTW (ResNet-18)	110	35	850	No (Strong GPU dependency)
Graph-TWFL (GNN)	210	60	1100	no

As shown in Table 3, this study examined the variations in computing efficiency while preserving excellent accuracy. The model in this research fully satisfies real-time localisation requirements with a GPU inference time of only 18 milliseconds. Additionally, a pure CPU takes 65 milliseconds, which is much faster than the 100 milliseconds that power systems usually need.

Table 4. Model Cross-Line Generalization Ability Test

Test line type	MAE (m)	Success rate (%)	Wave head recognition accuracy (%)
500 kV (same distribution)	162	98.5	99.1
220 kV (similar topology)	178	97.2	98.5
110 kV (short line)	195	95.8	97.6
±800 kV UHVDC	210	93.4	95.2
Urban power distribution network (including branches)	285	86.7	90.3

Table 4 examined the localization model's performance across topologies and its capacity to generalise at various voltage levels. The MAE very slightly increases at 220 kV and 110 kV, and the detection success rate surpasses 95%. This suggests that the model's learnt features are somewhat universal. Due to variations in sweepability and AC transmission techniques in intricate distribution network settings, performance in 800 kV DC circuits somewhat declines. Because there are no distinct branch pathways, the inaccuracy increases to 285 meters. This implies that in order to enhance the modelling of graph branches, the graph neural network module needs to be further expanded. The model exhibits strong transferability overall.

Table 5. Comparison of location performance under different fault types

Fault type	Sample size	SEA-TWFL MAE (m)	Two-End TW MAE (m)	Success rate increased (%)
Phase A grounded (R_f=0.1Ω)	300	150	170	+2.1
AB phase-to-phase	300	158	180	+1.8

short circuit				
ABC three-phase short circuit	300	145	165	+2.3
Phase A is grounded with high resistance (1000Ω).	300	210	520	+28.6
Phase B disconnection and grounding	300	195	310	+15.2
Intermittent arc grounding	300	230	480	+24.7

Table 5 analyzes the robustness of the model constructed in this paper under different types of faults, including high resistance, open circuit, and arcing. When the grounding resistance is 1000 ohms, the model's prediction error for different non-metallic problems is just 210 meters. When compared to techniques like the two-terminal method, this demonstrates a notable benefit. Traditional methods are particularly vulnerable to fault development in intermittent arcing faults due to the considerable amplitude of the wave variations and the irregularity of the travelling wave waveform. Nonetheless, the model presented in this study has a high success rate in capturing the wavefront during the first modelling process, suggesting that it is highly practical in a variety of complicated power grids.

5. Conclusion

An innovative technique for locating overhead line faults is presented in this research. A deep learning model that strikes a compromise between accuracy, robustness, and power engineering feasibility is built by integrating deep learning techniques, power expertise, and physical models. This model is tested under a variety of challenging conditions, such as long-distance lines and high-resistance faults. This approach provides a more economical and dependable solution than baseline models and conventional techniques that depend on communication synchronisation and reflected waves. This study mainly used PSCAD simulation data during the simulation process.Researchers in study did not, however, perform extensive testing using actual power grid waveform data. Moreover, many topologies and architectures, such as multi-branch T-junctions or hybrid overhead cable distribution scenarios, are not fully taken into account by the existing model. As a result, it is not very effective in solving these kinds of issues. In the future, the graph neural network module will be expanded to conduct generalised modelling for complex topologies, and real data from power grid businesses will be used for testing. To strike a compromise between accuracy and transparency, this study also employs interpretable embedding approaches.

It should be noted that only PSCAD simulation data were used for the experimental validation in this study. There may be differences between simulated travelling wave signals and actual field-recorded waveforms because of things like sensor bandwidth constraints, electromagnetic interference, and unknown line parameter variations, even though the simulation platform allows for precise control over fault parameters and environmental conditions. Accurately extracting wavefront arrival timings from field data, which frequently involves greater levels of noise and non-ideal waveform aberrations, is the main obstacle to moving from simulation to real-world engineering application. Future research will use real-world fault waveform recordings gathered from power grid operators for additional validation in order to address these problems, and transfer learning techniques will be used to improve the DWHN in order to close the domain gap. In order to improve the SEA-TWFL model's resilience and capacity for generalisation in real-world situations, online deployment techniques will also be investigated to gradually modify the model's parameters as new field data becomes available.

Declarations

Funding

This research did not receive any specific funding.

Competing Interests

The authors have declared that no competing interests exist.

Data Availability Statement

The data supporting the findings of this study are available within the article.

Author Contributions

Ju Yi conceptualization & Study Design; Peng Xu Statistical Analysis & methodology; Xiaopeng Lu Literature Search & validation, Shixu Liu investigation & software, Daijuan Wang data curation & writing—review and editing.

References

[1] Zhang XY, Xu BY, Han ZR, Shi F. Improvement of Traveling Wave-Based Fault Location Method for Overhead Distribution Lines. Protection and Control of Modern Power Systems. 2026;11(1):157-72. DOI: 10.23919/pcmp.2025.000040

[2] Wang YP, Xie LW, Liu F, Yu K, Zeng XJ, Bi LX, et al. Fault location method for distribution network considering distortion of traveling wavefronts. International Journal of Electrical Power & Energy Systems. 2024;159:11. DOI: 10.1016/j.ijepes.2024.110065

[3] Liu TQ, Zhang YH, Wang SL, Li XP, Gooi HB, Ghias A. Fault identification and fault location methods for VSC-HVDC transmission lines based on the traveling waveform difference. International Journal of Electrical Power & Energy Systems. 2023;147:13. DOI: 10.1016/j.ijepes.2022.108867

[4] Fayazi M, Joorabian M, Saffarian A, Monadi M. A single-ended traveling wave based fault location method using DWT in hybrid parallel HVAC/HVDC overhead transmission lines on the same tower. Electric Power Systems Research. 2023;220:17. DOI: 10.1016/j.epsr.2023.109302

[5] Wang XW, Zhang F, Wei XX, Gao J, Guo L, Wang YZ. Fault location of flexible grounding distribution system based on multivariate modes and kurtosis calibration. International Journal of Electrical Power & Energy Systems. 2023;150:10. DOI: 10.1016/j.ijepes.2023.109108

[6] Cheng L, Wang T, Wang Y. A novel fault location method for distribution networks with distributed generations based on the time matrix of traveling-waves. Protection and Control of Modern Power Systems. 2022;7(1):11. DOI: 10.1186/s41601-022-00265-8

[7] Zhang DH, Zhang WH, Wang CZ, Xiao XY. Fault Segment Location for MV Distribution System Based on the Characteristic Voltage of LV Side. Electronics. 2023;12(7):21. DOI: 10.3390/electronics12071734

[8] Elgamasy MM, Izzularab MA, Zhang XP. Single-End Based Fault Location Method for VSC-HVDC Transmission Systems. IEEE Access. 2022;10:43129-42. DOI: 10.1109/access.2022.3169777

[9] Wang XD, Gao X, Liu YM, Wang RJ, Ma N, Qu MN. Bi-level decision matrix based fault location method for multi-branch offshore wind farm transmission lines. International Journal of Electrical Power & Energy Systems. 2022;141:13. DOI: 10.1016/j.ijepes.2022.108137

[10] Jimenez-Aparicio M, Wilches-Bernal F, Reno MJ. Local, Single-Ended, Traveling-Wave Fault Location on Distribution Systems Using Frequency and Time-Domain Data. IEEE Access. 2023;11:74201-15. DOI: 10.1109/access.2023.3296737

[11] Wang D, Liu H, Zhang D, Qiao F, Liu XM, Hou MQ. Traveling wave fault location for LCC-MMC-MTDC transmission lines based on frequency-dependent characteristic. International Journal of Electrical Power & Energy Systems. 2022;138:8. DOI: 10.1016/j.ijepes.2021.107863

[12] Liu F, Xie LW, Yu K, Wang YP, Zeng XJ, Bi LX, et al. A novel fault location method based on traveling wave for multi-branch distribution network. Electric Power Systems Research. 2023;224:9. DOI: 10.1016/j.epsr.2023.109753

[13] Ren X, Feng ZQ, Zhou K, Zhou XM, Yuan JJ, Xu YF, et al. Improving Electrical Distance Accuracy for Cable Fault Location Based on the Prony Method. IEEE Access. 2025;13:135019-26. DOI: 10.1109/access.2025.3593833

[14] Hemmati M, Ghaffarzadeh N. A novel phaselet-based approach for fault detection and location in HVDC lines. Computers & Electrical Engineering. 2024;120:17. DOI: 10.1016/j.compeleceng.2024.109667

[15] Zhang C, Wang HY, Wang ZM, Li YD. Active detection fault diagnosis and fault location technology for LVDC distribution networks. International Journal of Electrical Power & Energy Systems. 2023;148:13. DOI: 10.1016/j.ijepes.2022.108921
[16] Sun GQ, Ma W, Wei SQ, Cai DF, Wang WZ, Xu CZ, et al. A Fault Location Method for Medium Voltage Distribution Network Based on Ground Fault Transfer Device. Electronics. 2023;12(23):13. DOI: 10.3390/electronics12234790
[17] Wang XW, Zhang F, Gao J, Guo L, Wang X, Liang ZF, et al. Fault location based on variable mode decomposition and kurtosis calibration in distribution networks. International Journal of Electrical Power & Energy Systems. 2023;154:10. DOI: 10.1016/j.ijepes.2023.109463
[18] Mousaviyan I, Seifossadat SG, Saniei M. Traveling Wave-based Algorithm for Fault Detection, Classification, and Location in STATCOM-Compensated Parallel Transmission Lines. Electric Power Systems Research. 2022;210:13. DOI: 10.1016/j.epsr.2022.108118
[19] Jia DL, Yang XY, He KY, Deng F, Wang ZT, Li TL. A Single-Ended Fault Location Method for DC Transmission Lines Based on Inverse Distance Weighted Interpolation. IEEE Access. 2025;13:147772-83. DOI: 10.1109/access.2025.3591637
[20] Su JA, Huang XW, Zhang P, Pang XH, Liang YW, Zhang LX, et al. Arc Fault Location for Photovoltaic Distribution Cables Based on Time Reversal. Symmetry-Basel. 2025;17(2):11. DOI: 10.3390/sym17020240
[21] Xie LW, Luo LF, Ma JJ, Li Y, Zhang MM, Zeng XJ, et al. A novel fault location method for hybrid lines based on traveling wave. International Journal of Electrical Power & Energy Systems. 2022;141:11. DOI: 10.1016/j.ijepes.2022.108102
[22] Wang YC, Li ZW, Chen ST, Zhang YM. Location Method of Single-Phase to Ground Fault in Distribution Network Based on Time-Frequency Matrix Analysis of Traveling Wave. Journal of Electrical Engineering & Technology. 2024;19(8):5221-33. DOI: 10.1007/s42835-024-02037-w
[23] Poursaeed AH, Namdari F. High-speed algorithm for fault detection and location in DC microgrids based on a novel time-frequency analysis. IET Generation Transmission & Distribution. 2024;18(24):4259-78. DOI: 10.1049/gtd2.13274
[24] Tariq R, Alhamrouni I, Rehman AU, Eldin ET, Shafiq M, Ghamry NA, et al. An Optimized Solution for Fault Detection and Location in Underground Cables Based on Traveling Waves. Energies. 2022;15(17):19. DOI: 10.3390/en15176468
[25] Luo XH, Deng ZM, Wu JY, Chen KY, Jia PJ. Fault nature identification and location scheme for distribution network based on active injection from IIDG. International Journal of Electrical Power & Energy Systems. 2024;156:10. DOI: 10.1016/j.ijepes.2023.109706